Title

Rapid sulfur cycling in sediments from the Peruvian oxygen minimum zone featuring simultaneous sulfate reduction and sulfide oxidation

Journal

Limnology and Oceanography, 66(7)

ISSN

0024-3590

Authors

Treude, Tina
Hamdan, Leila J
Lemieux, Sydnie
et al.

Publication Date

2021-07-01

DOI

10.1002/lno.11779

Peer reviewed

LIMNOLOGY and OCEANOGRAPHY

ASLO

Limnol. Oceanogr. 66, 2021, 2661–2671

doi: 10.1002/lno.11779

Rapid sulfur cycling in sediments from the Peruvian oxygen minimum zone featuring simultaneous sulfate reduction and sulfide oxidation

Tina Treude,[1,2*] **Leila J. Hamdan**,[3] **Sydnie Lemieux**,[2] **Andrew W. Dale**,[4] **Stefan Sommer**[4]

[1]Department of Earth, Planetary and Space Sciences, University of California, Los Angeles, California
[2]Department of Atmospheric and Oceanic Sciences, University of California, Los Angeles, California
[3]School of Ocean Science and Engineering, University of Southern Mississippi, Ocean Springs, Mississippi
[4]GEOMAR Helmholtz Centre for Ocean Research Kiel, Kiel, Germany

Abstract

Bacterial sulfate reduction (SR) is often determined by radiotracer techniques using ^{35}S-labeled sulfate. In environments featuring simultaneous sulfide oxidation, SR can be underestimated due to re-oxidation of ^{35}S-sulfide. Recycling of ^{35}S-tracer is expected to be high in sediment with low concentrations of pore-water sulfide and high abundance of giant filamentous sulfur-oxidizing bacteria (GFSOB). Here, we applied a sulfide-spiking method, originally developed for water samples, to sediments along a shelf-slope transect (72, 128, 243, 752 m water depth) traversing the Peruvian oxygen minimum zone. Sediment spiked with unlabeled sulfide prior to ^{35}S-sulfate injection to prevent radiotracer recycling was compared to unspiked sediment. At stations characterized by low natural sulfide and abundant GFSOB (128 and 243 m), the method revealed 1–3 times higher SR rates in spiked sediment. Spiking had no effect on SR in sediment with high natural sulfide despite presence of GFSOB (72 m). Bioturbated sediment devoid of GFSOB (752 m) showed elevated SR in spiked samples, likely from artificial introduction of sulfidic conditions. Sulfide oxidation rates at the 128 and 243 m station, derived from the difference in SR between spiked and unspiked sediment, approximated rates of dissimilatory nitrate reduction to ammonium by GFSOB. Gross SR contributed considerably to benthic dissolved inorganic carbon fluxes at the three shallowest station, confirming that SR is an important process for benthic carbon respirations within the oxygen minimum zone. We recommend to further explore the spiking method to capture SR in sediment featuring low sulfide concentrations and high sulfur cycling by GFSOB.

Bacterial sulfate reduction is the most important anaerobic metabolic process driving carbon remineralization in organic-rich, marine sediments (Jørgensen 1982; Canfield et al. 2005). In this respiratory process, sulfate serves as the terminal electron acceptor and is reduced to hydrogen sulfide after the following reaction:

$$2CH_2O + SO_4^{2-} \rightarrow 2HCO_3^- + H_2S \quad (1)$$

Note that CH_2O is an approximation of organic biomass with zero oxidation state and neglecting N, S, and P.

Knowledge of the magnitude of sulfate reduction, especially in sediment below productive environments featuring high organic matter export and the development of oxygen deficiency in the water column, is vital in understanding marine element cycling in the global ocean (Middelburg and Levin 2009; Treude 2011). In sediments underlying marine oxygen minimum zones (OMZs), organic matter degradation by sulfate reduction can be so vigorous to cause pelagic sulfidic events (Schunck et al. 2013) and to feed chemoautotrophic processes, such as the dissimilatory nitrate reduction to ammonium (DNRA) coupled to sulfur oxidation (Jørgensen and Nelson 2004; Høgslund et al. 2009), which can exhaust nitrate in the water column (Sommer et al. 2016). Pore-water sulfide is further an important regulator of iron fluxes into the anoxic water column and benthic pyritization in OMZs (Middelburg and Levin 2009).

A widely used method for determining sulfate reduction activity in sediments is the application of radiolabeled sulfate (^{35}S-sulfate) (Jørgensen 1978; Kallmeyer et al. 2004; Røy et al. 2014). After incubation with ^{35}S-sulfate, sediment is transferred to zinc acetate and frozen. The addition of zinc acetate stops evaporation of H_2S and terminates bacterial activity; freezing prevents chemical re-oxidation of sulfides (Røy et al. 2014). During analyses, total reduced inorganic sulfur (TRIS) is separated from residual ^{35}S-sulfate by either hot

*Correspondence: ttreude@g.ucla.edu

Author Contribution Statement: TT and LH conceptualised the study. TT, AWD and SS participated in the expedition and collected sediment samples. TT, LH, SL, and AWD conducted sediment analyses. SS planned and executed the expedition. TT wrote the manuscript with input from all co-authors.

(Jørgensen 1978) or cold (Kallmeyer et al. 2004) chromium distillation. Both methods provide quantitative information on sulfate reduction expressed as turnover of sulfate per sample volume or weight and time.

If, however, bacterial sulfide oxidation occurs simultaneously with sulfate reduction, gross sulfate reduction rates can be underestimated and partially masked, due to re-oxidation of produced ^{35}S-sulfide during incubation (Moeslund et al. 1994; Canfield et al. 2010; Findlay et al. 2020). This underestimation can be significant if the natural pool of sulfide in pore water is low, increasing the likelihood of re-oxidation of ^{35}S-sulfide that is released into the pore water during ^{35}S-sulfate incubation. Similarly, sulfate reduction rates can be underestimated when calculated by transport-reaction modeling of pore-water sulfate, as the in-situ sulfate concentration only reflects the sum of all redox and exchange processes (Fossing et al. 2000; Jørgensen et al. 2001; Treude et al. 2005).

Canfield et al. (2010) developed a method to unmask sulfate reduction during simultaneous sulfide oxidation in the water column of the Chilean OMZ. The method involved spiking water samples with unlabeled sulfide to increase the sulfide pool, thereby reducing likelihood of re-oxidation of the produced ^{35}S-sulfide by in-situ bacteria (Fig. 1B). Likewise, Fossing and Jørgensen (1990) spiked sediment with unlabeled thiosulfate prior to radiotracer injection to prevent fast turnover of ^{35}S-labeled thiosulfate, which is a short-lived intermediate in sulfur cycling. In the present study, we applied the sulfide-spiking method developed by Canfield et al. (2010) to sediments to study sulfate reduction and sulfide oxidation in benthic environments below the Peruvian OMZ. Sediments in this highly productive region are characterized by high rates of organic matter degradation (Dale et al. 2015), including sulfate reduction (Gier et al. 2016; Maltby et al. 2016), and the presence of giant filamentous sulfur-oxidizing bacteria (GFSOB), principally *Marithioploca* and *Beggiatoa* (Bohlen et al. 2011; Sommer et al. 2016; Dale et al. 2019). We studied benthic sulfate reduction along a depth transect (74–752 m) traversing the OMZ and found strong indications for rapid sulfur cycling in sediments inhabited by dense mats of GFSOB. The rapid cycling partially masked sulfate reduction activity determined by the traditional quantification method and likely prevented the buildup of hydrogen sulfide in the pore water. Our results provide new insights into the magnitude of sulfate reduction and sulfide oxidation in OMZ sediments. We further discuss the pros and cons of the application of the spiking method to sediments.

Materials and methods

Study area

Detailed description of the study area can be found in previous studies (Mosch et al. 2012; Dale et al. 2015; Sommer

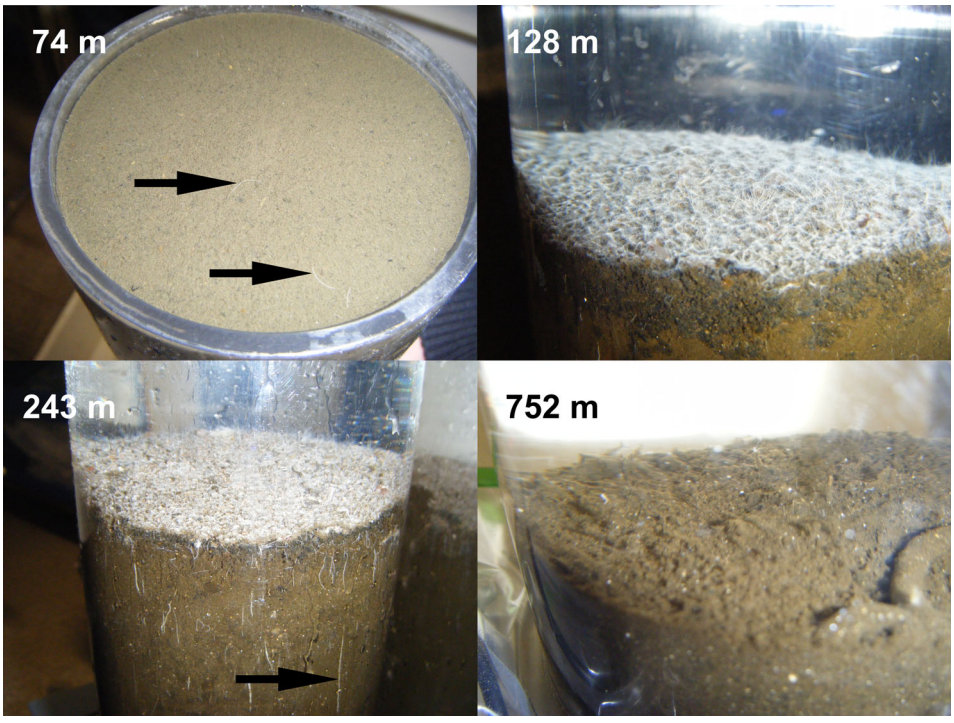

Fig 1. Photographs of representative sediment multicorer cores taken at the four sampling stations: 74, 128, 243, and 752 m. Cores were photographed within 30 min after recovery and immediately before sub-sampling. Arrows in the photograph from the 74 m station point to individual filaments of giant sulfur bacteria visible at the sediment surface. The arrow in the photograph from the 243 m station points to a vertically oriented sulfur bacteria sheath inside the sediment. The internal diameter of the core liners was 10 cm. For details, see "Sediment Sampling" section.

et al. 2016; Lüdke et al. 2020) and references therein. The 12° S depth transect on the Peruvian margin, the setting of the present study, is located within a pronounced OMZ. The OMZ is sustained by heterotrophic microbial respiration coupled to enhanced organic carbon export from a highly productive surface ocean. Primary production is driven by nutrient-rich upwelling sustained by alongshore equatorward trade winds and cyclonic wind-stress curl (Strub et al. 1998). The core of the OMZ, exhibiting dissolved oxygen concentration below detection limit of the Winkler titration (5 μM), intersects with the seafloor at water depths between 100 and 500 m (Dale et al. 2015; Sommer et al. 2016), while oxygen concentrations on the shelf (in particular < 100 m) vary seasonally and show intra-annual variability (Graco et al. 2017; Lüdke et al. 2020). Previous work on the 11° S transect through the OMZ revealed that epibenthic megafauna were virtually absent between approximately 70 and 400 m, reaching highest abundance (e.g., gastropods: 900 indiv. m^2, ophiuroids: 140 indiv. m^2, and pennatulaceans: 20 indiv. m^2) between the lower OMZ boundary (460 m) and 680 m (Mosch et al. 2012). Carbon remineralization based on dissolved inorganic carbon fluxes in the sediment decrease from $\sim$ 80 mmol C m^{-2} d^{-1} at 74 m to $\sim$ 3 mmol C m^{-2} d^{-1} at 756 m (Dale et al. 2015). Oxygen deficiency in the water column shifts organic matter degradation in sediment to anaerobic processes, supplying sediments with hydrogen sulfide generated by dissimilatory sulfate reduction (Bohlen et al. 2011; Gier et al. 2016; Sommer et al. 2016). The released hydrogen sulfide serves as an energy source for GFSOB mats (Bohlen et al. 2011; Sommer et al. 2016). These mats couple sulfide oxidation to the DNRA, leading to high benthic ammonium fluxes (Bohlen et al. 2011; Sommer et al. 2016). Seafloor observations with a towed camera confirmed GFSOB mats at the sediment–water interface at water depths between 70 and 300 m (Mosch et al. 2012; Sommer et al. 2016). Trichomes of GFSOB extended into the overlying water by 1–2 cm and were visible down to ca. 20 cm below the seafloor (cmbsf) (Dale et al. 2016). Abundance of mats fluctuate in time at shallower depths (< 100 m) as a result of nitrate and oxygen concentration variability (Gutiérrez et al. 2008; Dale et al. 2016; Sommer et al. 2016).

Sediment sampling

Sediment samples were taken between April and May 2017 during two consecutive expeditions on research vessel (R/V) *Meteor* (M136 and M137) at four stations (74, 128, 243, and 752 m) along the 12° S depth transect traversing the Peruvian OMZ. Samples were retrieved using a TV-guided multicorer (MUC) equipped with seven core liners as described previously (Dale et al. 2016). Core liners were 60 cm long with an inner diameter of 10 cm. Filaments of GFSOB were observable by eye at the sediment surface (dense mat) and inside sediment at the 128 and 243 m stations (Fig. 1; Sommer et al. 2019). Filaments were detected mostly inside sediment at the 74 m station and were not observed at the 752 m station. Retrieved cores were immediately transferred to cold rooms (12°C) for further processing. Station and sampling details, including deployment positions, for the studied parameters are provided in Table 1. Note that due to logistical reasons samples for different analyses were collected from replicate MUC deployments.

Sulfate reduction rates

At each station, two small push cores (length 20 cm, inner diameter 2.6 cm) were subsampled from one MUC core. One of the replicate sub-cores (hereafter "spiked core") was amended with unlabeled sulfide: 16 μL saturated sulfide solution (2.42 M stock solution: 250 g $Na_2S \bullet 9\ H_2O$ in 420 mL ultrapure water) was injected into the sediment push core through pre-drilled holes placed at 1 cm depth increments following the principle of the whole-round core injection method (Jørgensen 1978). Based on an average sediment water content of $\sim$ 80% (Gier et al. 2016; Maltby et al. 2016), the added sulfide resulted in a final sulfide concentration of 10 mM in the pore water after its dilution into the sediment (5 cm^3 sediment per injection point). The second sub-core remained untreated (hereafter "unspiked core"). After an equilibration for 1–2 h at 12°C in the dark, 10 μL of carrier-free $^{35}SO_4^{2-}$ radiotracer (dissolved in water, 1.86 MBq, specific activity 37 TBq $mmol^{-1}$) was injected into both sub-cores at 1 cm depth increments according to the whole-core injection method (Jørgensen 1978). In the spiked core, radiotracer was injected through the same ports used for sulfide injection. Both spiked and unspiked cores were incubated with radiotracer for 6–8 h at 12°C in the dark.

After incubation, bacterial activity was stopped by slicing sub-cores at 1 cm increments and transferring sediment layers into 50 mL plastic centrifuge tubes filled with 20 mL zinc acetate (20% w/w). Triplicate "killed" controls were produced from additional sediment of the same MUC core and microbial activity was first terminated with zinc acetate before the addition of radiotracer to the centrifuge vial. All samples were frozen at −20°C until analysis, when sulfate reduction rates were determined following the cold chromium distillation procedure (Kallmeyer et al. 2004). Sulfate reduction rates are reported per volume (cm^3) and integrated over depth (0–5 and 0–15 cmbsf). Integrated spiked rates were divided by integrated unspiked rates to calculate a sulfate reduction rate ratio (SRR ratio). An SRR ratio > 1 indicates excess spiked rates, while an SRR ratio < 1 indicates excess unspiked rates.

Geochemical analyses

Geochemical analyses served to understand the distribution of key parameters involved in sulfur cycling and to provide essential parameters (sulfate concentration and porosity) for sulfate reduction rate calculations. Pore-water extraction and analysis and the determination of sediment properties are described in Dale et al. (2015). In short, one MUC core per deployment was subsampled for pore water under anoxic

Table 1. Details of stations selected for this study along the 12°S depth transect.

Average water depth (m)	Station no.	MUC no.	Expedition	O_2 concentration close to seafloor (μmol kg^{-1})*	Latitude	Longitude	Date	Parameters collected
74	681	13	M137	bdl-12	12°13.51′S	77°10.78′W	12 May 2017	SR
	721	22	M137		12°13.47′S	77°10.80′W	15 May 2017	NO_3
	483	8	M136		12°13.52′S	77°10.79′W	24 Apr 2017	Sulfate, sulfide, TA, ammonium, porosity
128	771	27	M137	bdl	12°16.73′S	77°14.95′W	19 May 2017	SR
	426	6	M136		12°16.68′S	77°14.95′W	19 Apr 2017	Sulfate, sulfide, TA, ammonium, porosity
243	775	31	M137	bdl	12°23.29′S	77°24.28′W	19 May 2017	SR
	751	26	M137		12°24.00′S	77°24.28′W	17 May 2017	NO_3
	595	1	M137		12°23.30′S	77°24.28′W	06 May 2017	Sulfate, sulfide, TA, ammonium, porosity
752	670	12	M137	16	12°31.36′S	77°35.00′W	11 May 2017	SR
	543	9	M136		12°31.35′S	77° 35.01′W	28 Apr 2017	Sulfate, sulfide, TA, ammonium, porosity

bdl, below detection limit; MUC, multicorer; TA, total alkalinity.
*Data collected with a lowered SeaBird SBE 9-plus conductivity-temperature-depth (CTD) system using two pumped oxygen sensors (Lüdke et al. 2020).

conditions using an argon-filled glove bag. Ammonium (NH_4^+) and total sulfide concentrations were analyzed on a Hitachi U2800 UV/VIS spectrophotometer using standard photometric procedures (Grasshoff et al. 1999). The detection limit for both solutes was 1 μM and the precision of the analyses was 5 μM. Sulfate (SO_4^{2-}) concentrations were determined by ion chromatography (Metrohm 761) with a detection limit of $< 100\,\mu$M and precision of 200 μM. Total alkalinity was determined by direct titration of 1 mL pore water with 0.02 M HCl using a mixture of methyl red and methylene blue as an indicator and bubbling the titration vessel with argon gas to strip CO_2 and hydrogen sulfide. The analysis was calibrated using IAPSO seawater standard, with a precision and detection limit of 0.05 meq L^{-1}. A second core from the same MUC deployment was sampled to determine porosity by the weight difference of the fresh sediment before and after freeze drying. Porosity data are not presented and served only for the calculation of sulfate reduction rates (*see* Kallmeyer et al. 2004). A third core from a separate MUC deployment was taken for determination of total nitrate (NO_3^-) in the sediment. For this, the upper 5 cm of the core was sliced in 1 cm intervals, repeatedly frozen and thawed to burst intracellular vacuoles of GFSOB and foraminifera, then centrifuged at 3000 × *g* for 20 min, and analyzed according to Dale et al. (2016). Analysis of the filtered pore water gives the biological nitrate stored within vacuolated organisms as well as any pore-water nitrate present.

Results

Sulfate reduction

At the 74 m station, sulfate reduction in the top 1 cmbsf (centimeter below sea floor) of the unspiked core was more than double than in the spiked core (962 vs. 379 nmol cm^{-3} d^{-1} respectively, Fig. 2A). Below 1 cmbsf, rates declined in both cores and tracked between cores, especially below 5 cmbsf, where rates ranged between 40 and 60 nmol cm^{-3} d^{-1}.

At the 128 m station, sulfate reduction in the spiked core declined from 106 nmol cm^{-3} d^{-1} at 0–1 cmbsf to ~ 15 nmol cm^{-3} d^{-1} below 8 cmbsf (Fig. 2D). Sulfate reduction in the top 5 cmbsf of the spiked core was always 30–40 nmol cm^{-3} d^{-1} higher than in the unspiked core. Below 5 cmbsf, the difference between the two cores became less pronounced with depth, and rates were almost identical below 8 cmbsf.

At the 243 m station, sulfate reduction in the spiked core peaked at 0–1 cmbsf (56 nmol cm^{-3} d^{-1}), dropped sharply to 25 nmol cm^{-3} d^{-1} at 0–2 nmol cm^{-3} d^{-1}, subsequently steadily declining to 4.3 nmol cm^{-3} d^{-1} at the deepest depth (15–16 cmbsf). Sulfate reduction in the top 5 cmbsf of the spiked core was consistently 15–20 nmol cm^{-3} d^{-1} higher than in the unspiked core (Fig. 2G). Below 5 cmbsf, this difference declined to 5–10 nmol cm^{-3} d^{-1}. Only at the deepest sampled depth (15–16 cmbsf), did both cores reach equal rates.

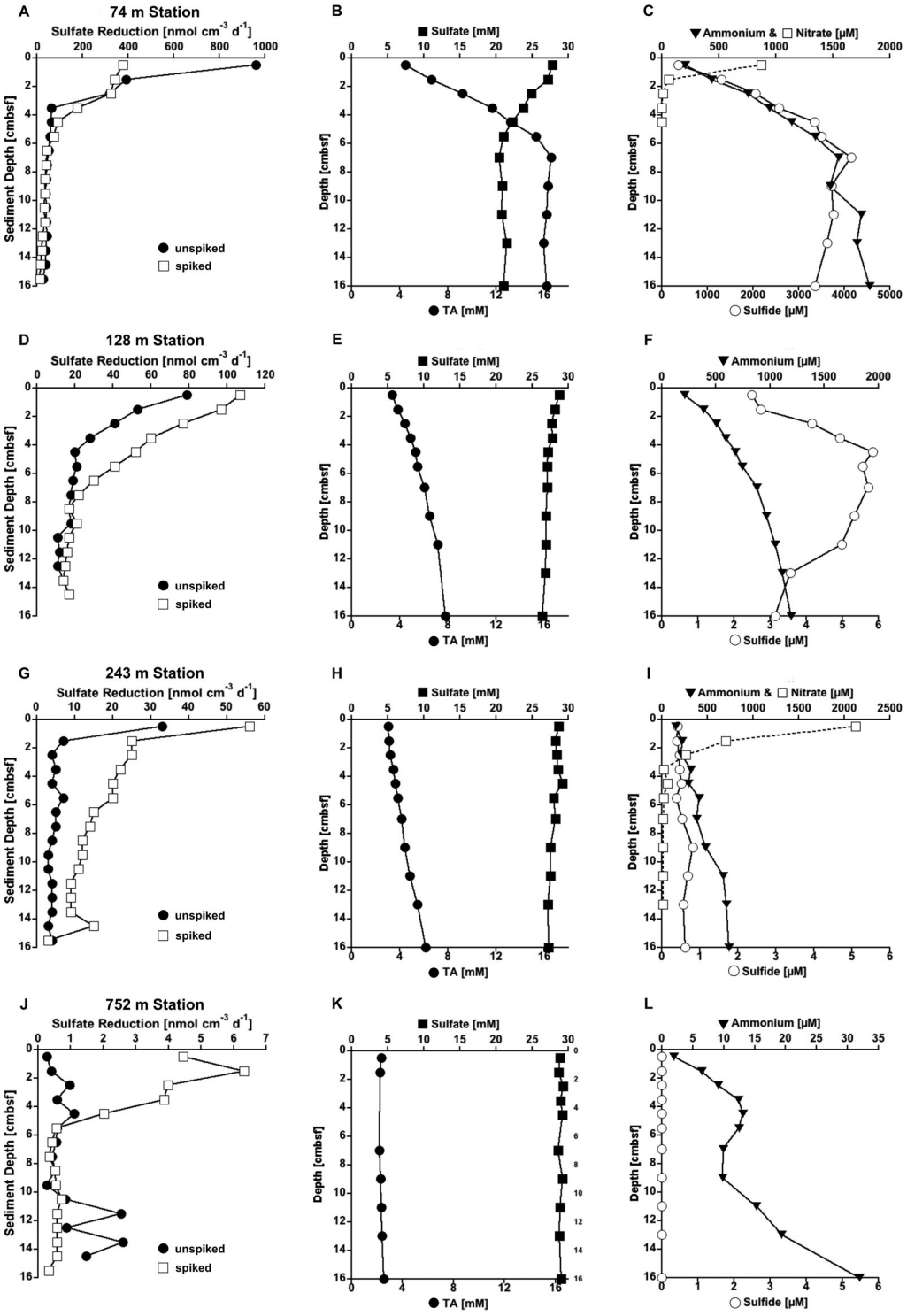

Fig 2. Depth profiles of biogeochemical parameters determined at the four stations (74, 128, 243, and 752 m). (**A**, **D**, **G**, **J**): Sulfate reduction in sulfide-spiked and unspiked sediment cores. (**B**, **E**, **H**, **K**): Concentrations of sulfate (SO_4^{2-}) and total alkalinity (TA) in the pore water. (**C**, **F**, **I**, **L**): Concentrations of ammonium (NH_4^+), total nitrate (NO_3^-), and total sulfide in the pore water. Note that total nitrate data are not available for the 128 and 752 m station.

At the 752 m station, sulfate reduction in the spiked core ranged between 2.0 and 6.3 nmol cm^{-3} d^{-1} above 5 cmbsf and declined to 0.3–0.7 nmol cm^{-3} d^{-1} below (Fig. 2J). Sulfate reduction in the top 5 cmbsf of the spiked core was between 1 and 6 nmol cm^{-3} d^{-1} higher than in the unspiked core. From 5 to 11 cmbsf rates of both cores agreed. Below 11 cmbsf, sulfate reduction in the unspiked core was 0.3–2 nmol cm^{-3} d^{-1} higher than the spiked core and was variable.

Sulfate reduction rates integrated over depth (0–15 cmbsf) declined two orders of magnitude with water depth between the 74 and the 752 m station, in both the unspiked and spiked core (Table 2). The SRR ratio was < 1 at the 74 m station and > 1 at the other stations, showing the highest ratio at the 243 m station, followed by the 752 and the 128 m station (Table 2).

Pore-water geochemistry

At the 74 m station, sulfate declined from 27.8 mM at 0–1 cmbsf (hereafter referred to "top") to 21.1 mM at 4–5 cmbsf. Below 5 cmbsf, values remained relatively constant around 21 mM (Fig. 2B). The trend of total alkalinity, which serves as an indicator for anaerobic degradation of organic matter under oxygen-deficient conditions and associated secondary redox reactions (Gustafsson et al. 2019), was opposite to sulfate, showing an increase from 5.5 mM at the top to ~ 16 mM below 5 cmbsf. Total nitrate was highest at the top (871 μM) and sharply decreased with depth reaching levels ~ 2 μM at 3–4 cmbsf and below. Ammonium and sulfide both increased sharply from 206 and 357 μM at the top to 1549 and 4147 μM at 6–8 cmbsf, respectively (Fig. 2C). Below 8 cmbsf, ammonium increased, and sulfide decreased only slightly. It is notable that this station had by far the highest sulfide concentrations and the strongest decline in sulfate compared to the other three stations.

At the 128 m station, sulfate showed a slight concave downward decrease from 28.8 mM at the top to 26.4 mM at 14–18 cmbsf (bottom) (Fig. 2E). The profile of total alkalinity showed a concave downwards increase from 3.40 mM at the top to 7.79 mM at the bottom. Ammonium showed a strong concave downwards increases with depth from 210 μM at the top to 1193 μM at the bottom (Fig. 2F). Sulfide was relatively low (between 2 and 6 μM) compared to the 74 m station, featuring peaks between 4 and 7 cmbsf. Total nitrate is not available for this station.

At the 243 m station, sulfate concentration changed very little (from 28.7 to 27.3 mM) from the top to the bottom of the core (Fig. 2H). Total alkalinity showed a linear increase from 3.06 mM at the top to 6.10 mM at the bottom. Total nitrate reached a very high concentration (2123 μM) at the top, sharply declined but remained high (> 200 μM) between 1 and 3 cmbsf and reached levels of 10–50 μM at 3–10 cmbsf. Ammonium and sulfide both increased from top to bottom in serrated profiles (Fig. 2I). Ammonium reached a maximum of 740 μM at the bottom. Sulfide levels remained below the technical detection limit (1 μM) throughout the core.

At the 752 m station, sulfate stayed close to seawater concentration (28 mM) throughout the core (Fig. 2K). Total alkalinity showed no notable change with depth and remained ~ 2.4 mM throughout the core. Ammonium reached a maximum of 31.9 μM at the bottom and featured an S-shaped bend in the profile between 4 and 10 cmbsf (Fig. 2L). No sulfide was detected in the pore water. Total nitrate is not available for this station.

Depth-integrated sulfate reduction vs. nitrate inventory

The depth-integrated (0–5 cmbsf) total nitrate inventory in the sediment after freeze/thawing (Table 2) was compared with depth-integrated sulfate reduction in spiked cores (0–5 cmbsf, expressed as SRR ratio, Table 2). A positive correlation of the nitrate inventory in the pore water with a high SRR ratio indicates the presence of GFSOB with vacuolated nitrate storage conducting sulfide oxidation (compare with Fossing et al. 1995; Preisler et al. 2007). Note that cells of nitrate-reducing foraminifera could be a potential additional source of nitrate in the sediment (Glock et al. 2019). Nitrate data from M137 were combined with data from M92 (Dale et al. 2016) to close sampling gaps (Table 2). Samples from M92 were sampled from the same stations and treated in the same way as samples from M137. It is noted, however, that annual and seasonal variabilities between the M92 and M137 expedition are conceivable. The linear regression plot of the two variables (SRR ratio vs. nitrate inventory) for the three shallowest stations (74, 128, 243 m) indicated a positive correlation between excess spiked sulfate reduction (SRR ratio > 1) and nitrate inventory ($R^2 = 0.78$, Fig. 3). However, the correlation was not significant (p-value = 0.118), due to the low number of replication ($n = 5$). No total nitrate data are available for the 752 m station, although intracellular nitrate is expected to be negligible since vacuolated GFSOB were visually absent during core slicing and sulfate reduction was 1–2 orders of magnitude lower compared to shallower stations.

We further tested if sulfate reduction in the zone of high total nitrate (0–5 cmbsf) differed significantly between spiked and unspiked cores (independent Student's t-test). For this calculation, the five 1-cm layers of each core were treated as replicates. No significant difference between spiked and unspiked sulfate reduction was found for the 74 m station (p-value = 0.295), while sulfate reduction at the 128 and 243 m station differed significantly (p-value = 0.024 and 0.032, respectively).

Discussion

Comparison of sulfate reduction rates in sulfide-spiked vs. unspiked sediments

Both sulfide-spiked and unspiked sulfate reduction determinations revealed a decrease in sulfate reduction rates with increasing water depth, concomitant with the decrease of

particulate organic carbon flux to the seafloor along the transect (Dale et al. 2015). Spiking with sulfide, however, showed individual effects on sulfate reduction that were uncorrelated with water depth. Sulfate reduction at stations with high visual abundance of GFSOB (station 128 and 243 m, Fig. 1 and Sommer et al. 2019) displayed 1.6 and 2.8 times higher depth-integrated (0–15 cmbsf) sulfate reduction rates, respectively, in spiked as in unspiked sediments (Table 2). This difference was significant (p-value = 0.024 and 0.032, respectively) in the top 5 cm. Presence of GFSOB was further supported by the high nitrate inventory at these stations (Fig. 3), suggesting substantial storage of nitrate in vacuoles of GFSOB. The addition of non-labeled sulfide prior to ^{35}S-sulfate injection therefore likely strongly limited the re-oxidation of produced ^{35}S-sulfide by sulfide oxidizers, and thereby unmasked an otherwise undetected fraction of sulfate reduction.

The 74 m station differed from the 128 and 243 m station in several ways: (1) sulfate reduction was about one order of magnitude larger (Fig. 2A,D,G), (2) sulfate showed a more pronounced decline with depth (Fig. 2B,E,H), (3) pore-water sulfide concentrations were 3–4 orders of magnitude higher (Fig. 2C,F,I), and (4) the nitrate inventory was lower (Fig. 3). We therefore suggest that the addition of sulfide did not cause additional preservation of ^{35}S-sulfide due to high initial sulfide concentration and lower sulfide-oxidation activity. It is notable that the 25% difference in depth-integrated (0–15 cmbsf) sulfate reduction rates at this station was caused by a single large peak in sulfate reduction rate in the top (0–1 cmbsf) sediment layer of the unspiked sediment (Fig. 2A). The reason for the peak is unknown but could be caused by patchiness of organic matter deposition from the water column (Wakeham et al. 1984). However, despite the higher activity at 0–1 cmbsf in the unspiked core, the statistical test did not detect a significant difference (p-value = 0.295) in activity between the cores in the top 5 cm.

A strong positive effect of sulfide addition on sulfate reduction was found at the 752 m station. Here, depth-integrated (0–15 cmbsf) sulfate reduction was 1.9 times as much as the spiked core, mostly due to elevated turnover in the top 5 cmbsf. This station was characterized by $\sim 16\ \mu M\ O_2$ in the water column above the seafloor (Table 1), the presence of epibenthic megafauna indicative of sediment bioturbation (compare also with Mosch et al. 2012), and visual absence of GFSOB (Fig. 1). Vertical profiles of pore-water sulfate and total alkalinity, absence of sulfide, and non-linear ammonium profiles are further indications of bioturbation activity in sediment. It is therefore possible that the addition of sulfide provided a sink for oxygen, nitrate, and metal oxides, and thereby shifted organic matter degradation to sulfate reduction. In addition, sulfate reduction in anoxic micro-niches of the unspiked core could have been partially masked due to oxidation of ^{35}S-sulfide to ^{35}S-S° by reactive iron and coupled oxidation or disproportionation of ^{35}S-S° to ^{35}S-sulfate by microbial processes (Findlay et al. 2020). Microbial disproportionation of S° is thermodynamically feasible at sulfide concentrations < 1 mM (Thamdrup et al. 1993), which was provided in the sediment of the 752 m station. Generally, spiking with "cold" sulfide will suppress all pathways from labeled sulfide to labeled sulfate, regardless of the mechanism.

Table 2. Depth-integrated sulfate reduction rates (unspiked and sulfide-spiked) and nitrate inventory at the four stations. SRR ratio = spiked/unspiked sulfate reduction. Depth-integrated sulfate reduction rates and ratios are shown for 0–15 and (in brackets) for 0–5 cm. Depth-integrated nitrate inventories are shown for 0–5 cm, and expeditions M92 and M137. For more details, see text.

Station	Sulfate reduction			Nitrate inventory	
	Unspiked	Spiked	SRR ratio	M92	M137
	(mmol m^{-2} d^{-1})			(mmol m^{-2})	
74 m	22.5 (18.0)	16.8 (13.2)	0.75 (0.73)	5.1	8.8
128 m	3.80 (2.21)	6.02 (3.92)	1.58 (1.77)	30.6	
243 m	0.973 (0.550)	2.76 (1.48)	2.83 (2.69)	23.6	30.2
752 m	0.141	0.261	1.85	n.d.	n.d.

n.d., not determined.

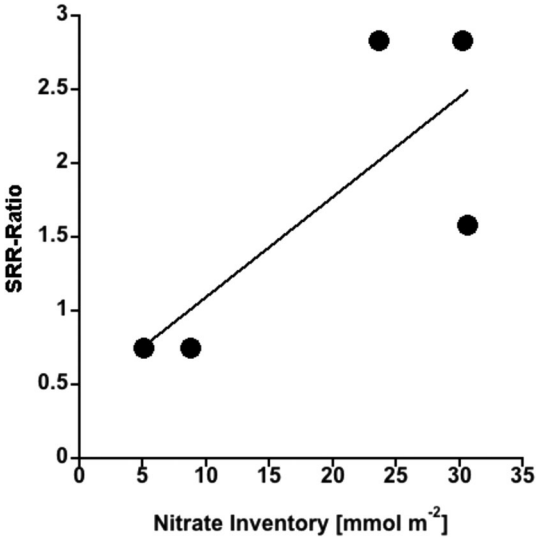

Fig 3. SRR ratio vs. nitrate inventory. Black line displays linear regression (R^2 = 0.78, p-value = 0.118). SRR ratio = spiked sulfate reduction divided by unspiked sulfate reduction (depth-integrated rates, 0–5 cmbsf). Nitrate inventory = the sum of vacuolated and pore water nitrate (depth-integrated, 0–5 cmbsf). Note that the 5–10 cmbsf depth section did not show significant concentrations of nitrate in any cores and was therefore excluded from integration. Data for nitrate were combined from two expeditions (M92 and M137). For more details, see Table 2 and text.

Evaluation of the method application to sediment

In the present study, the sulfide-spiking method, which was developed by Canfield et al. (2010) to uncover sulfate

reduction in waters with fast sulfur cycling, was applied to sediment cores. The results suggest that the difference in sulfate reduction between the spiked and the unspiked cores represents the partial or full rate of simultaneous sulfide-oxidation. Note that some of the sulfide oxidation could be masked by the formation of ^{35}S intermediates (S°, polysulfides), which would analytically be attributed to sulfate reduction due to their conversion to ^{35}S-H_2S during the cold-chromium distillation (Kallmeyer et al. 2004; Røy et al. 2014).

In contrast, sulfide spiking did not uncover additional sulfate reduction in anoxic sediments with high sulfide concentrations at the 74 m station. Here, ^{35}S-sulfide re-oxidation was likely already minimized by the naturally high sulfide pool. At the 752 m station, sulfide spiking potentially stimulated sulfate reduction in oxidized sediments by creating reduced conditions. Consequently, to accurately assess the impact of sulfide reoxidation on sulfate reduction, it is advisable to combine spiked with non-spiked incubations and to include geochemical analyses such as sulfide, sulfate, and nitrate to interpret the results.

Sulfide injection did not cause noticeable negative effects on sulfate reduction through sulfide toxicity. The calculated final sulfide concentration (10 mM) after diffusion into pore water was below concentrations observed, for example, at cold seeps (up to 26 mM) in the presence of active sulfate reduction (Sahling et al. 2002; Treude et al. 2003); however, local sulfide concentration created immediately after the injections of 2.42 M stock solution, must have been temporarily significantly higher, and also caused a strong increase in pH. At the 128 and 243 m stations, GFSOB apparently responded fast to the additional sulfide pool, potentially alleviating toxic sulfide levels and high pH. At the 752 m station, a larger fraction of sulfide was likely consumed in chemical reactions with metal oxides. Potential buffers for sulfide toxicity are not clear for the 74 m station, since conditions in sediment were already reducing (Fig. 2C) and sulfur cycling was not efficient (*see* discussion above).

With the recent introduction of a ^{35}S-sulfide-labeling technique to directly determine sulfide oxidation rates in sediments (Findlay et al. 2020), the advantages and disadvantages of this technique vs. the sulfide-spiking method presented here is worth a short discussion. It should be kept in mind that the ^{35}S-sulfide-labeling technique was developed to quantify total sulfide oxidation rates, while the sulfide-spiking method in combination with ^{35}S-sulfate labeling aims at quantifying total sulfate reduction rates. The ^{35}S-sulfide-labeling technique has proven useful in oxidized, iron-rich sediments, while our results show that the spiking method potentially stimulates artificial sulfate reduction in such environments through the introduction of reduced (sulfidic) conditions. The sensitivity of the ^{35}S-sulfide-labeling technique decreases with increasing sulfide concentration due to label dilution, while the spiking method does not alter the result at high sulfide concentrations, although its application under these conditions is not necessary. Both techniques only capture sulfide oxidation that ends in the production of sulfate, thereby potentially underestimating sulfide oxidation to S°, which is an important intermediate stored in the cells of GFSOB (Jørgensen and Nelson 2004). In summary, depending on the aim of the study, the above two methods can be applied (separately or in combination) to serve different purposes.

Implications for sulfur cycling in Peruvian OMZ sediments

Benthic fluxes of dissolved inorganic carbon, determined by in-situ chamber deployments during the M92 expedition, were 65.9, 20.4, 4.7, and 2.8 mmol m^{-2} d^{-1} at the 74, 128, 243, and 752 m station, respectively (Dale et al. 2015). Dissolved inorganic carbon flux was assumed to originate from particulate organic carbon remineralization with negligible effects of carbonate precipitation and dissolution. Relative to the dissolved inorganic carbon fluxes, depth-integrated sulfate reduction (0–15 cmbsf, unspiked/spiked) in our study amounted to 68/51, 37/59, 41/117, and 10/19%, respectively, of particulate organic carbon remineralization at these stations (compare with Table 2; Eq. 1). Note that sulfate reduction from the spiked core at the 752 m station is likely an overestimation (*see* discussion above). These percentages suggest that sulfate reduction constituted an important part of carbon remineralization at the three shallowest stations within the OMZ, while it was accomplished mostly by other processes, such as aerobic respiration, denitrification, ion/manganese reduction, at the deepest station.

Benthic ammonium fluxes attributed to DNRA by GFSOB during M92 at the 128 and 243 m station were 2.0–6.7 and 0.6–0.7 mmol NH_4^+ m^{-2} d^{-1}, respectively (Sommer et al. 2016). During DNRA, equal molar amounts of sulfide and ammonium are consumed and produced, respectively (Zopfi et al. 2001). Considering the different methods applied (benthic flux chambers for DNRA vs. radiotracer technique for sulfur cycling), ammonium fluxes show a reasonable match with depth-integrated (0–15 cmbsf) sulfide oxidation rates derived from the difference between spiked and unspiked sulfate reduction (2.2 and 1.8 mmol sulfide m^{-2} d^{-1} at the 128 and 243 m station, respectively; compare with Table 2). Similarly, modeled nitrate reduction via DNRA (5.5 and 1.1 mmol NO_3^- m^{-2} d^{-1} at 128 and 243 m, respectively) was in the same order of magnitude (Dale et al. 2016). However, note that sulfide oxidation rates could be underestimated for reasons discussed in the method evaluation section.

At the 752 m station, a relatively low contribution of sulfate reduction to organic carbon remineralization was not surprising, considering that the seafloor intersected with oxygenated water (Table 1) and was rich in benthic fauna (compare with Mosch et al. 2012), which can bioirrigate electron acceptors more attractive than sulfate deeper into the sediment (Krantzberg 1985; Kristensen 2000). At this station, benthic oxygen consumption rates yielded up to

1.4 mmol m^{-2} d^{-1} (Sommer et al. 2016) in comparison to 0.14 and 0.26 mmol m^{-2} d^{-1} sulfate reduction (Table 2). With increasing water depth, i.e., decreasing particulate organic carbon flux, aerobic respiration, and denitrification become progressively more important for organic carbon remineralization in sediments (Orcutt et al. 2013).

Conclusion

The sulfide-spiking method developed by Canfield et al. (2010), which was applied here to sediments, produced higher rates of sulfate reduction and reasonable rates of sulfide oxidation in sediments from the Peruvian OMZ that featured both (1) a high abundance of GFSOB and (2) a low concentration of pore-water sulfide. Our data suggest that determination of sulfate reduction with ^{35}S- radiotracer in sediments featuring rapid sulfide re-oxidation can lead to rate underestimation in traditional incubations without sulfide spiking. We therefore recommend to further test the applicability of this method to produce realistic sulfate reduction rates in benthic environments with active sulfur cycling such as organic-rich sediments (e.g., Preisler et al. 2007; Bertics et al. 2013; Valentine et al. 2016; Findlay et al. 2020) and cold seeps (e.g., Joye et al. 2004; Niemann et al. 2006; Treude et al. 2003). Improving the quantification of sulfate reduction rates in sediments will be beneficial, e.g., for reaction modeling of early diagenesis—in particular in low-oxygen environments.

Data Availability Statement

Datasets are accessible via the PANGAEA data base under the following DOIs:

Sulfate reduction: https://doi.org/10.1594/PANGAEA.930403

Freeze/thaw nutrients: https://doi.org/10.1594/PANGAEA.918339

Geochemistry 595 MUC 1: https://doi.pangaea.de/10.1594/PANGAEA.923171

Geochemistry 426 MUC 6: https://doi.pangaea.de/10.1594/PANGAEA.922510

Geochemistry 483 MUC 8: https://doi.pangaea.de/10.1594/PANGAEA.922514

Geochemistry 543 MUC 9: https://doi.pangaea.de/10.1594/PANGAEA.922518

References

Bertics, V. J., and others. 2013. Occurrence of benthic microbial nitrogen fixation coupled to sulfate reduction in the seasonally hypoxic Eckernfoerde Bay, Blatic Sea. Biogeosciences **10**: 1243–1258.

Bohlen, L., and others. 2011. Benthic nitrogen cycling traversing the Peruvian oxygen minimum zone. Geochim. Cosmochim. Acta Theriol. **75**: 6094–6111.

Canfield, D. E., B. Thamdrup, and E. Kristensen. 2005. Aquatic Geomicrobiology. Elsevier.

Canfield, D. E., and others. 2010. A cryptic sulfur cycle in oxygen-minimum–zone waters off the Chilean coast. Science **330**: 1375–1378.

Dale, A. W., and others. 2015. Organic carbon production, mineralisation and preservation on the Peruvian margin. Biogeosciences **12**: 1537–1559.

Dale, A. W., S. Sommer, U. Lomnitz, A. Bourbonnais, and K. Wallmann. 2016. Biological nitrate transport in sediments on the Peruvian margin mitigates benthic sulfide emissions and drives pelagic N loss during stagnation events. Deep-Sea Res. I Oceanogr. Res. Pap. **112**: 123–136.

Dale, A. W., A. Bourbonnais, M. Altabet, K. Wallmann, and S. Sommer. 2019. Isotopic fingerprints of benthic nitrogen cycling in the Peruvian oxygen minimum zone. Geochim. Cosmochim. Acta **245**: 406–425.

Findlay, A. J., A. Pellerin, K. Laufer, and B. B. Jørgensen. 2020. Quantification of sulphide oxidation rates in marine sediment. Geochim. Cosmochim. Acta **280**: 441–452.

Fossing, H., and B. B. Jørgensen. 1990. Oxidation and reduction of radiolabeled inorganic sulfur compounds in an estuarine sediment, Kysing Fjord, Denmark. Geochim. Cosmochim. Acta **54**: 2731–2742.

Fossing, H., and others. 1995. Concentration and transport of nitrate by the mat-forming sulphur bacterium Thioploca. Nature **374**: 713–715.

Fossing, H., T. G. Ferdelman, and P. Berg. 2000. Sulphate reduction and methane oxidation in continental sediments influenced by irrigation (south-east Antlantik off Namibia). Geochim. Cosmochim. Acta **64**: 897–910.

Gier, J., S. Sommer, C. R. Löscher, A. W. Dale, R. A. Schmitz, and T. Treude. 2016. Nitrogen fixation in sediments along a depth transect through the Peruvian oxygen minimum zone. Biogeosciences **13**: 4065–4080.

Glock, N., and others. 2019. Metabolic preference of nitrate over oxygen as an electron acceptor in foraminifera from the Peruvian oxygen minimum zone. Proc. Natl. Acad. Sci. **116**: 2860–2865.

Graco, M. I., and others. 2017. The OMZ and nutrient features as a signature of interannual and low-frequency variability in the Peruvian upwelling system. Biogeosciences **14**: 4601–4617.

Grasshoff, K., M. Ehrhardt, and K. Kremling. 1999. Methods of seawater analysis. Wiley-VCH Verlag GmbH.

Gustafsson, E., and others. 2019. Sedimentary alkalinity generation and long-term alkalinity development in the Baltic Sea. Biogeosciences **16**: 437–456.

Gutiérrez, D., and others. 2008. Oxygenation episodes on the continental shelf of Central Peru: Remote forcing and benthic ecosystem response. Prog. Oceanogr. **79**: 177–189.

Høgslund, S., and others. 2009. Physiology and behaviour of marine Thioploca. ISME J. **3**: 647–657.

Jørgensen, B. B. 1978. A comparison of methods for the quantification of bacterial sulphate reduction in coastal marine sediments: I. Measurements with radiotracer techniques. Geomicrobiol. J. **1**: 11–27.

Jørgensen, B. B.1982. Mineralization of organic matter in the sea bed - the role of sulphate reduction. Nature **296**: 643–645.

Jørgensen, B. B., A. Weber, and J. Zopfi. 2001. Sulphate reduction and anaerobic methane oxidation in Black Sea sediments. Deep-Sea Res. I **48**: 2097–2120.

Jørgensen, B. B., and D. C. Nelson. 2004. Sulfide oxidation in marine sediments: Geochemistry meets microbiology. Geol. Soc. Am. Spec. Pap. **379**: 63–81.

Joye, S. B., and others. 2004. The anaerobic oxidation of methane and sulfate reduction in sediments from Gulf of Mexico cold seeps. Chem. Geol. **205**: 219–238.

Kallmeyer, J., T. G. Ferdelman, A. Weber, H. Fossing, and B. B. Jørgensen. 2004. A cold chromium distillation procedure for radiolabeled sulfide applied to sulfate reduction measurements. Limnol. Oceanogr. Methods **2**: 171–180.

Krantzberg, G. 1985. The influece of bioturbation on physical, chemical, and biological parameters in aquatic environments: A review. Environ. Pollut. **39**: 99–122.

Kristensen, E. 2000. Organic matter diagenesis at the oxic/anoxic interface in coastal marine sediments, with emphasis on the role of burrowing animals. Hydrobiologia **426**: 1–24.

Lüdke, J., Dengler, M., Sommer, S., Clemens, D., Thomsen, S., Krahmann, G., Dale, A. W., Achterberg, E. P. and Visbeck, M. 2020. Influence of intraseasonal eastern boundary circulation variability on hydrography and biogeochemistry off Peru. Ocean Science **16**: 1347–1366.

Maltby, J., S. Sommer, A. W. Dale, and T. Treude. 2016. Microbial methanogenesis in the sulfate-reducing zone of surface sediments traversing the Peruvian margin. Biogeosciences **13**: 283–299.

Middelburg, J. J., and L. A. Levin. 2009. Coastal hypoxia and sediment biogeochemistry. Biogeosciences **6**: 1273–1293.

Moeslund, L., B. Thamdrup, and B. B. Jørgensen. 1994. Sulfur and iron cycling in a coastal sediment: Radiotracer studies and seasonal dynamics. Biogeochemistry **27**: 129–152.

Mosch, T., and others. 2012. Factors influencing the distribution of epibenthic megafauna across the Peruvian oxygen minimum zone. Deep-Sea Res. I Oceanogr. Res. Pap. **68**: 123–135.

Niemann, H., and others. 2006. Novel microbial communities of the Haakon Mosby mud volcano and their role as a methane sink. Nature **443**: 854–858.

Orcutt, B. N., and others. 2013. Microbial activity in the marine deep biosphere: Progress and prospects. Front. Microbiol. **4**: 189.

Preisler, A., D. De Beer, A. Lichtschlag, G. Lavik, A. Boetius, and B. B. Jørgensen. 2007. Biological and chemical sulfide oxidation in a Beggiatoa inhabited marine sediment. ISME J.: **1**: 341–351.

Røy, H., H. S. Weber, I. H. Tarpgaard, T. G. Ferdelman, and B. B. Jørgensen. 2014. Determination of dissimilatory sulfate reduction rates in marine sediment via radioactive 35S tracer. Limnol. Oceanogr. **12**: 196–211.

Sahling, H., D. Rickert, W. L. Raymond, P. Linke, and E. Suess. 2002. Macrofaunal community structure and sulfide flux at gas hydrate deposits from the Cascadia convergent margin, NE Pacific. Mar. Ecol. Prog. Ser. **231**: 121–138.

Schunck, H., and others. 2013. Giant hydrogen sulfide plume in the oxygen minimum zone off Peru supports chemolithoautotrophy. PLOS ONE **8**: e68661.

Sommer, S., and others. 2016. Depletion of oxygen, nitrate and nitrite in the Peruvian oxygen minimum zone cause an imbalance of benthic nitrogen fluxes. Deep-Sea Res. I **112**: 113–122.

Sommer, S., M. Dengler, and S. S. Party. 2019. Benthic element cycling, fluxes and transport of nutrients and trace metals across the benthic boundary layer in the Peruvian oxygen minimum zone (SFB 754), Cruise No. 137, 06.05. - 29.05.2017, Callao (Peru) - Callao, p. 52.

Strub, P. T., J. M. Mesías, V. Montecino, J. Rutllant, and S. Salina. 1998. Coastal ocean circulation off western South America, p. 273–313. *In* A. R. Robinson and K. H. Brink [eds.], The sea, v. **11**. Harvard University Press.

Thamdrup, B., K. Finster, J. W. Hansen, and F. Bak. 1993. Bacterial disproportionation of elemental sulfur coupled to chemical reduction of iron and manganese. Appl. Environ. Microbiol. **59**: 101–108.

Treude, T., A. Boetius, K. Knittel, K. Wallmann, and B. B. Jørgensen. 2003. Anaerobic oxidation of methane above gas hydrates at hydrate ridge, NE Pacific Ocean. Mar. Ecol. Prog. Ser. **264**: 1–14.

Treude, T., and others. 2005. Anaerobic oxidation of methane in the sulfate-methane transition along the Chilean continental margin. Geochim. Cosmochim. Acta Theriol. **69**: 2767–2779.

Treude, T. 2011. Biogeochemical reactions in marine sediments underlying anoxic water bodies, p. 18–38. *In* A. Altenbach, J. Bernhard, and J. Seckbach [eds.], Anoxia: Paleontological strategies and evidence for eukaryote survival. Cellular origins, life in extreme habitats and astrobiology (COLE) book series. Springer.

Valentine, D. L., and others. 2016. Autonomous marine robotic technology reveals an expansive benthic bacterial community relevant to regional nitrogen biogeochemistry. Environ. Sci. Technol. **50**: 11057–11065.

Wakeham, S. G., J. W. Farrington, and R. B. Gagosian. 1984. Variability in lipid flux and composition of particulate matter in the Peru upwelling region. Org. Geochem. **6**: 203–215.

Zopfi, J., T. Kjær, L. P. Nielsen, and B. B. Jørgensen. 2001. Ecology of *Thioploca* spp.: Nitrate and sulfur storage in relation to chemical microgradients and influence of *Thioploca* spp.

on the sedimentary nitrogen cycle. Appl. Environ. Microbiol. **67**: 5530–5537.

Acknowledgments

This study was funded by the Deutsche Forschungsgemeinschaft as part of the Sonderforschungsbereich 754 "Climate–Biogeochemistry Interactions in the Tropical Ocean." Further support came from the University of California, Los Angeles (Faculty Research Grant). The authors thank the Peruvian authorities for the permission to carry out scientific work in their national waters. The authors thank the captains and the crew of R/V Meteor for their support during the cruises. The authors thank Bettina Domeyer, Anna Plaß, Florian Scholz, and Regina Surberg for geochemical pore-water analyses and Kathleen Knight for support during the sulfate reduction analyses. This manuscript benefitted from comments by B.B. Jørgensen and J. Kallmeyer.

Conflict of interest

None declared.

Submitted 02 November 2020
Revised 05 February 2021
Accepted 06 April 2021

Associate editor: Florence Schubotz